

Mode identification of Pulsating White Dwarfs using the HST ¹

S.O. Kepler

Instituto de Física, Universidade Federal do Rio Grande do Sul, 91501-970 Porto Alegre, RS –
Brazil

E.L. Robinson

McDonald Observatory and Department of Astronomy, The University of Texas, Austin, TX
78712-1083 – USA

D. Koester

Institut für Astronomie und Astrophysik, Universität Kiel, D-24098 Kiel, Germany

J.C. Clemens

Department of Physics, University of North Carolina, Chapel Hill, NC 27599-3255 – USA

R.E. Nather

McDonald Observatory and Department of Astronomy, The University of Texas, Austin, TX
78712-1083 – USA

and

X. J. Jiang

Beijing Astronomical Observatory and United Laboratory of Optical Astronomy, Chinese
Academy of Sciences, Beijing 100101, China

Received 31 Jan 2000; accepted 17 Mar 2000

Submitted to Ap.J.

¹Based on observations with the NASA/ESA Hubble Space Telescope, obtained at the Space Telescope Science Institute, which is operated by the Association of Universities for Research in Astronomy, Inc. under NASA contract No. NAS5-26555

ABSTRACT

We have obtained time-resolved ultraviolet spectroscopy for the pulsating DAV stars G226–29 and G185–32, and for the pulsating DBV star PG1351+489 with the Hubble Space Telescope Faint Object Spectrograph, to compare the ultraviolet to the optical pulsation amplitude and determine the pulsation indices. We find that for essentially all observed pulsation modes, the amplitude rises to the ultraviolet as the theoretical models predict for $\ell = 1$ non-radial g-modes. We do not find any pulsation mode visible only in the ultraviolet, nor any modes whose phase flips by 180° in the ultraviolet, as would be expected if high ℓ pulsations were excited. We find one periodicity in the light curve of G185–32, at 141 s, which does not fit theoretical models for the change of amplitude with wavelength of g-mode pulsations.

Subject headings: stars: white dwarfs, stars: variables, stars, individual: G226-29, G185-32, PG1351+489

1. 1. Introduction

Observations of white dwarf stars are an important probe of stellar and galactic evolution. The properties of individual white dwarfs define the endpoints for models of stellar evolution, while the white dwarf luminosity function provides an observational record of star formation in our galaxy. For example, the coolest normal-mass white dwarfs are remnants of stars formed in the earliest epoch of star formation, so their cooling times can tell us the age of the galactic disk in the solar neighborhood (Winget et al. 1987, Wood 1992) and the effects of phase separation and crystallization at extreme densities (Chabrier et al. 1992, Segretain et al. 1994, Winget et al 1997).

As the number of pulsation modes detected in the pulsating white dwarfs is insufficient for an inverse solution of the structure of the star, we must identify the pulsation modes to compare with the theoretical models and infer the structural parameters.

A crucial step in determining the structure of a white dwarf from its pulsation periods is to identify the pulsation modes correctly. The pulsation modes in our models are indexed with three integers (k, ℓ, m) where k represents the number of nodes in the pulsation eigenfunction along the radial direction, ℓ is the total number of node lines on the stellar surface, and m is the number of node lines passing through the pulsation poles. Pulsation modes with different indices generally have different pulsation periods. The usual procedure for identifying the mode indices is (1) calculate theoretical pulsation periods in models of white dwarfs; (2) compare the pattern of theoretical periods to the observed pattern of periods; (3) adjust the models to bring the theoretical and observed patterns into closer agreement. The problems with this procedure are clear: it does not work for white dwarfs with only a few excited pulsation modes, as it places too few constraints on the stellar structure; and, given the complexity and sophistication of the theoretical calculations and the large number of possible pulsation modes, there is ample opportunity to misidentify modes. Other methods of mode identification must be used to avoid these problems.

2. Mode Identification Using Time-Resolved UV Spectroscopy

Time-resolved ultraviolet spectroscopy provides an independent method for determining the pulsation indices of white dwarfs. The amplitudes of g -mode pulsations depend strongly on ℓ at wavelengths shorter than 3000 Å. Figure 1 shows how the amplitude depends on wavelength and ℓ for the lowest-order modes of pulsating white dwarfs. The amplitude of all modes increases towards the ultraviolet but the amplitude increases more for $\ell = 2$ than for $\ell = 1$. The differences are even greater for modes with higher ℓ . Note the predicted 180° phase flip of the $\ell = 4$ mode for the DAV models at wavelengths shorter than 1500Å, indicated by the negative amplitudes.

The increase in amplitude from optical to ultraviolet wavelengths is caused by two effects: the increasing effect of the temperature on the flux, and the increasing effect of limb darkening in the ultraviolet. The differences among the amplitudes of modes with different ℓ are caused mainly by limb darkening. The brightness variations of non-radially pulsating white dwarfs are due entirely to variations in effective temperature; geometric variations are negligible (Robinson, Kepler, & Nather 1982). The normal modes divide the stellar surface into zones of higher and lower effective temperature that can be described by spherical harmonics; modes of higher ℓ have more zones than those of lower ℓ . From a distance, we can measure only the integrated surface brightness, which includes the effects of limb darkening, so modes of high ℓ are normally washed out by the cancellation of different zones. But at ultraviolet wavelengths, the effects of limb darkening increase drastically, decreasing the contribution of zones near the limb. Consequently, modes of higher ℓ are cancelled less effectively in the UV and their amplitudes increase more steeply at short wavelengths than those of low ℓ . Theoretical calculations of the amplitudes require good model atmospheres but are entirely independent of the details of pulsation theory and white dwarf structure calculations.

Robinson et al. (1995) used this method to determine ℓ for the pulsating DA white dwarf G117–B15A. They measured the amplitude of its 215 s pulsation in the ultraviolet with the HST high-speed photometer and identified it as an $\ell = 1$ mode. With the correct value of ℓ , they found that the mass of the surface hydrogen layer in G117–B15A was between 1.0×10^{-6} and

$8 \times 10^{-5} M_{\odot}$, too thick to be consistent with models invoking thin hydrogen layers to explain the spectral evolution of white dwarfs. They also found $T_{\text{eff}} = 12\,375 \pm 125$ K, substantially lower than the accepted temperature at that time, but close to the presently accepted temperature (Koester et al. 1994, Bergeron et al. 1995, Koester & Allard 2000).

To extend these results, we observed the pulsating DA white dwarfs G226–29 (DN Dra) and G185–32 (PY Vul), and the DBV PG1351+489 (EM UMa) with 10 sec/exposure RAPID mode of the (now decommissioned) Faint Object Spectrograph (FOS) of the Hubble Space Telescope. We used the blue Digicon detector and the G160L grating over the spectral region 1150 Å to 2510 Å.

3. Observations

3.1. G226–29

G226–29, also called DN Dra, LP 101 – 148, and WD 1647+591, is the brightest known pulsating DA white dwarf (DAV or ZZ Ceti star), with $m_v = 12.22$. At a distance of just over 12 pc, it is the closest ZZ Ceti star (optical parallax of 82.7 ± 4.6 mas, Harrington & Dahn 1980; Hipparcos parallax of 91.1 ± 2.1 mas, Vauclair et al. 1997). Its pulsations were discovered by McGraw & Fontaine (1980), using a photoelectric photometer attached to the MMT telescope. They found a periodicity at 109 s with a 6 mma (mili modulation amplitude) amplitude near 4200 Å. Kepler, Robinson, & Nather (1983) used time-series photometry to solve the light curve and interpret the variations as an equally spaced triplet with periods near 109 s. The outer peaks have similar amplitudes, near 3 mma, and are separated by a frequency $\delta f = 16.14 \mu\text{Hz}$ from the central peak, which has an amplitude of 1.7 mma. These results were confirmed by Kepler et al. (1995a), using the Whole Earth Telescope, who also showed that no other pulsation were present with amplitudes larger than 0.4 mma. G226–29 has the simplest mode structure, the second smallest overall pulsation amplitude, and the shortest dominant period of any pulsating white dwarf.

For G226–29, the very short (109 s) period triplet leads to a seismological interpretation of

the structure by Fontaine et al. (1994), who show the star should have a thick hydrogen layer ($\log q = \log M_{\text{H}}/M_{\star} = -4.4 \pm 0.2$) if the observed triplet is the rotationally split $\ell = 1$, $k = 1$ mode. Kepler et al. (1995a), assuming an $\ell = 1$, $k = 1$ triplet, also derived an hydrogen layer mass about $10^{-4}M_{\star}$. Higher k values would imply an unreasonably thick hydrogen layer.

Several recent spectroscopic studies show G226–29 to be one of the hottest of the ZZ Ceti stars, suggesting that we may be observing it as it enters the instability strip. The absolute effective temperature of this star is not settled, because one can derive two different effective temperatures for a given gravity using optical spectra, and also because there are uncertainties about the best convective efficiency to use in model atmospheres (Bergeron et al. 1992, 1995, Koester & Vauclair 1997). Fontaine et al. (1992) derive $T_{\text{eff}} = 13,630 \pm 200$ K and $\log g = 8.18 \pm 0.05$, corresponding to a stellar mass of $0.70 \pm 0.03M_{\odot}$, based on high signal-to-noise optical spectra and ML2/ $\alpha = 1$ model atmospheres. This effective temperature places G226–29 near the blue edge of their ZZ Ceti instability strip. Kepler & Nelan (1993) used published IUE spectra and optical photometry to derive $T_{\text{eff}} = 12\,120 \pm 11$ K, assuming $\log g = 8.0$; their ZZ Ceti instability strip is much cooler, $12\,640 \text{ K} \geq T_{\text{eff}} \geq 11\,740 \text{ K}$.

Koester & Allard (1993) use the Lyman α line profile to derive a parallax-consistent solution of $T_{\text{eff}} = 12\,040$ K and $\log g = 8.12$. Bergeron et al. (1995) found $T_{\text{eff}} = 12\,460$, and $\log g = 8.29$ for an $\alpha = 0.6$ ML2 model which fits the IUE and optical spectra simultaneously; their instability strip spans $12\,460 \geq T_{\text{eff}} \geq 11\,160$ K, placing G226–29 on the blue edge. Koester, Allard & Vauclair (1995) show G226–29 must have nearly the same temperature as L 19–2 and G117–B15A, at about 12 400 K, in agreement with Kepler & Nelan (1993), Koester & Allard (1993), and Bergeron et al. (1995). Kepler et al. (1995b) found $T_{\text{eff}} = 13\,000 \pm 110$, and $\log g = 8.19 \pm 0.02$, which corresponds to a mass of $0.73 M_{\odot}$, from the optical spectra alone, using Bergeron’s ML2 model atmosphere. Giovannini et al. (1998), using the same optical spectra as Kepler et al., but using Koester’s ML2 model atmosphere, obtained $T_{\text{eff}} = 13\,560 \pm 170$, and $\log g = 8.09 \pm 0.07$, which corresponds to a mass of $0.66 M_{\odot}$, for a DA evolutionary model of Wood (1995). Koester & Allard (2000) obtained $T_{\text{eff}} = 12\,050 \pm 160$ K, and $\log g = 8.19 \pm 0.13$, using IUE spectra, V magnitude

and parallax. This general agreement on the value of $\log g$ suggests the mass is around $0.70M_{\odot}$. The effective temperature is most probably 12 100 K, consistent with the IUE continuum, parallax and optical line profiles simultaneously.

G226–29 was observed with the HST six times, each time for 3 hours, between September 1994 and December 1995. As the star is bright and fairly hot, the time-averaged spectrum from the total of 18.6 hrs of observation has a high signal-to-noise ratio (Figure 2).

3.2. G185–32

The largest-amplitude pulsations of G185–32 have periods of 71 s, 141 s and 215 s (McGraw et al. 1981). We observed G185–32 with HST for a total of 7.1 hr on 31 Jul 1995. The Fourier transform of the UV and Zeroth order (see section 4) light curve (Figure 3) shows the periods we have identified for this star.

3.3. PG1351+489

PG1351+489 is the DBV with the simplest pulsation spectrum, and therefore the one which requires the shortest data set to measure its amplitude. Its pulsations, discovered by Winget, Nather & Hill (1987), have a dominant period at 489 s and a peak-to-peak blue amplitude near 0.16 mag. The light curve also shows the first and second harmonics of the this period (f_0), plus peaks at $1.47 f_0$, $2.47 f_0$ and $3.47 f_0$, with lower amplitudes. We observed PG1351+489 for 4 consecutive orbits of HST, for a total of 2.67 hr. The ultraviolet and Zeroth order (see section 4) Fourier spectra (Figure 4) show only the 489 s period and its harmonic at 245 s above the noise, and a possible period at 599 s.

4. Zeroth Order Data

Although not much advertised by the STScI, the zeroth order (undiffracted) light from an object falls onto the FOS detector when using the G160L grating and provides simultaneous photometry of the object with an effective wavelength around 3400 Å (see Figure 5) (Eracleous & Horne 1996).² The simultaneous photometry from the zeroth order light was crucial to the success of this project. As the zeroth order light has a counting rate around 100 times larger than the total light collected in the first order time resolved spectra, it can also be used to search for low amplitude pulsations. In the searched range of 800 s to 20 s, no new ones were found for any star observed in this project, to a limit around 8 mma.

The calibration pipeline of the HST data contains a transmission curve for the zeroth order data measured on the ground prior to launch (Figure 6), but our data are inconsistent with this transmission curve. We will discuss this later in section 9.

5. Data Set Problems

We detected two significant problems in the FOS data sets on G226–29, the first star we observed. First, we found a $\sim 3\%$ modulation of the total count rate on a time scale similar to the HST orbital period (see Figure 7). This modulation is probably caused by a combination of factors. We used a 1 arcsec entrance aperture and a triple peak-up procedure to center the star in the aperture for the first 5 observations. The triple peak-up process yields a centering accuracy of only ± 0.2 arcsec which, when coupled with the 0.8 arcsec PSF of the image, produces light loss at the edges of the aperture of at least a few percent. As the position of the star image in the aperture wanders during the HST orbit, the amount of light lost at the aperture varies, modulating the detected flux.

The second problem became evident when we compared the observed spectrum to the

²The data can be extracted from pixels 620 to 645 from the c4 files.

spectrum of G226–29 obtained with IUE and to model atmospheres for DA white dwarfs (Koester, Allard & Vauclair 1994). We found a spurious “bump” in the FOS spectrum in a 75 Å region just to the blue of 1500 Å. The bump is not subtle: it rises 25% above the surrounding continuum (see Kepler, Robinson & Nather 1995).

The excess was caused by a scratch on the cathode of the FOS blue detector, in a region used only for the G160L grating, for which the pipeline flat field did not correct properly. The scratch is at an angle with respect to the diode array so that the wavelength of the bump in the spectrum changes as the position of the spectrum on the cathode changes. The pipeline flat field was obtained with a 0.04 arcsec centering accuracy in the 4.3 arcsec aperture and is not accurate for any other aperture or position. For our sixth and last observation, we used the upper 1.0 pair aperture to minimize the flat fielding problem. A method for re-calibrating all post-COSTAR observations with the G160L has recently been devised, including an Average Inverse Sensitivity correction.³ After re-calibration, there was significant improvement in our data, but there is still some problem with the flux calibration redwards of 2200Å, as well as some scattered light into the Ly α core.

To identify the pulsation modes in a white dwarf we need to know only the fractional amplitudes of the pulsations as a function of wavelength. As the fractional amplitudes are immune to multiplicative errors in the calibration of the spectrograms, and as both problems we found are multiplicative, these problems do not affect our results. Data for wavelengths shorter than 1400 Å have known scattered light correction problems which, being additive, reduce the accuracy of our measured amplitudes by an uncertain amount.

³The AIS should be used with STSDAS task calfos, using the FLX_CORR omit option.

6. Models

The model atmospheres used to fit the time-averaged spectra, and to calculate the intensities at different angles with the surface normal, were calculated with a code written by Koester (Finley, Koester, Basri 1997). The code uses the $ML2/\alpha=0.6$ version of the standard mixing length theory of convection and includes the latest version of the quasi-molecular Lyman α opacity after Allard et al. (1994). This choice of convective efficiency allows for a consistent temperature determination from optical and ultraviolet time-average spectra (Bergeron et al. 1995, Vauclair et al. 1997, Koester & Allard 2000). $ML2/\alpha = 0.6$ is also consistent with the wavelength dependence of the amplitude observed in G117–B15A by Robinson et al. (1995), according to Fontaine et al. (1996).

To calculate the amplitudes of the pulsations, we require the specific intensities emitted by the white dwarf atmospheres as a function of wavelength, emitted angle, effective temperature, gravity, and chemical composition.

Robinson, Kepler & Nather (1982) calculated the luminosity variations of g-mode pulsations, and Robinson et al. (1995) expanded the results to include explicitly an arbitrary limb darkening law $h_\lambda(\mu)$, where $\mu = \cos\theta$. If we call the coordinates in the frame of pulsation (r, Θ, Φ) , the coordinates in the observer’s frame (r, θ, ϕ) , and assume

$$r = R_o(1 + \epsilon \xi_r)$$

with

$$\xi_r = \text{Real}\{Y_{\ell m}(\Theta, \Phi)e^{i\sigma t}\}$$

and assume low amplitude adiabatic pulsations

$$\frac{\delta T}{T} = \nabla_{ad} \frac{\delta P}{P},$$

then the amplitude of pulsation at wavelength λ , $A(\lambda)$, defined as

$$A(\lambda) \cos \sigma t = \frac{\Delta F(\lambda)}{F(\lambda)}$$

is given by

$$A(\lambda) = \epsilon Y_{\ell m}(\Theta_0, 0) \left(\frac{1}{I_{0\lambda}} \frac{\partial I_{0\lambda}}{\partial T} \right) \left(R_0 \frac{\delta T}{\delta r} \right) \times \frac{\int h_\lambda(\mu) P_\ell(\mu) \mu d\mu}{\int h_\lambda(\mu) \mu d\mu} \quad (1)$$

where $I_{0\lambda}$ is the sub-observer intensity, i.e., the intensity for $\cos\theta = 1$, and $P_\ell(\mu)$ are the Legendre polynomials. We have defined $(\Theta_0, 0)$ as the coordinates of the observer’s $\theta = 0$ axis with respect to the (r, Θ, Φ) coordinate system.

By taking the ratio $A(\lambda)/A(\lambda_0)$, we can eliminate the perturbation amplitude ϵ , the effect of the inclination between the observer’s line of sight and the pulsation axis [$Y_{\ell m}(\Theta_0, 0)$], and the term $R_0(\delta T/\delta r)$, all of which cancel out. The term $\left(\frac{1}{I_{0\lambda}} \frac{\partial I_{0\lambda}}{\partial T}\right)$ and the limb darkening function $h_\lambda(\mu)$ must be calculated by the model atmosphere code, and the amplitude ratio is then calculated by numerical integration. For g-mode pulsations, the amplitude ratio is therefore a function of ℓ .

7. Fit to the Time Averaged Spectra

For G226–29, we used our high S/N average spectra to fit to Koester’s model atmospheres, constrained by HIPPARCOS parallax (Vauclair et al. 1997) to obtain $T_{\text{eff}} = 12\,000 \pm 125$ K, $\log g = 8.23 \pm 0.05$. The pure spectral fitting does not significantly constrain $\log g$, but confines T_{eff} to a narrow range. The parallax, on the other hand, very strongly constrains the luminosity, and (via the mass-radius relation and T_{eff}) also the radius, and thus $\log g$ (Figure 8).

For G185–32, Koester & Allard (2000) also show that the V magnitude and the parallax can be used to constraint the gravity and they obtained $\log g = 7.92 \pm 0.1$ and $T_{\text{eff}} = 11\,820 \pm 110$ K. Our time-averaged HST spectrum (Figure 9) gives an effective temperature value of $T_{\text{eff}} = 11\,770 \pm 30$ K, for such surface gravity. The time-averaged HST spectra alone cannot, for any star studied here, constrain both the effective temperature and the surface gravity simultaneously, and that is the main reason the parallax is used when available, as a further constraint.

For PG1351+489, whose spectra is shown in Figures 10 and 11, we don’t have a parallax measurement, and pure He models give similar fit for $\log g = 7.50$ and $T_{\text{eff}} = 24\,090 \pm 620$ K, or $\log g = 7.75$ and $T_{\text{eff}} = 24\,000 \pm 210$ K, or $\log g = 8.00$ and $T_{\text{eff}} = 23\,929 \pm 610$ K. Our quoted values are for pure helium atmosphere, but to complicate things further, Beauchamp et al (1999) can fit the optical spectra with $T_{\text{eff}} = 26\,100$ K, $\log g = 7.89$ for pure helium model, but $T_{\text{eff}} = 22\,600$ K,

$\log g = 7.90$ allowing some hydrogen, undetectable in the optical spectra.

8. Optical Data for G226–29

Since most of the ground-based time-series observations to date on G226–29 were obtained in white light with biakali photocathode detectors, we obtained simultaneous UBVR time series photometry using the Stiening photometer (Robinson et al. 1995) attached to the 2.1 m Struve telescope at McDonald Observatory, in March to June 1995, for a total on 39.2 hr of 1 sec exposures on the star. We then transformed the time base to Barycentric Julian Dynamical Time (BJDD) to eliminate the phase shift introduced by the motion of the Earth relative to the barycenter of the solar system. We calculated a Fourier transform of the intensity versus time, for each of the UBVR colors, and measured the amplitudes and phases for the three modes, called P_0 , P_1 , and P_2 , the triplet around 109 s (Table 1). Even though we use this nomenclature, we are *not* assuming the three modes correspond to an $\ell = 1$ mode split by rotation, as we are studying the ℓ value for each component independently. Mode P_0 has a period of 109.27929 s, P_1 has a period of 109.08684 s, P_2 has a period of 109.47242 s. The phases of the three modes are the same in all filters, as expected for g -mode pulsations (Robinson, Kepler & Nather 1982).

As the HST data on G226–29 were spread out over 16 months, the ephemeris of our previous optical data were not accurate enough to bridge the resulting time gaps, requiring us to obtain an additional optical data set to improve the accuracy of the pulsation ephemeris. We observed the star again with the McDonald Observatory 2.1 m telescope for 1.7 hr from 8–15 May 96, 1.4 hr on 7 Feb 97, 2.7 hr on 6 May 1997, and 13.6 hr from 3 Jun 1997 to 11 Jun 1997 using the 85cm telescope at Beijing Astronomical Observatory with a Texas 3 star photometer. With this data set we were able to improve the ephemeris for the three pulsations enough to cover the HST data set and, using the 1995 data set, to extend back to the 1992 Whole Earth Telescope data set. Our new ephemeris, accurate from 1992 to 1997, is:

$$P_0 = 109.279\,299\,45\text{ sec} \pm 3.3 \times 10^{-6}\text{ sec},$$

$$T_{\max}^0(\text{BJDD}) = 244\,8678.789\,330\,34 \pm 3.7 \text{ sec};$$

$$P_1 = 109.086\,874\,54 \text{ sec} \pm 1.8 \times 10^{-6} \text{ sec},$$

$$T_{\max}^1(\text{BJDD}) = 244\,8678.789\,951\,19 \pm 2.0 \text{ sec};$$

$$P_2 = 109.472\,385\,02 \text{ sec} \pm 6.5 \times 10^{-7} \text{ sec},$$

$$T_{\max}^2(\text{BJDD}) = 244\,8678.789\,541\,96 \pm 0.5 \text{ sec}.$$

Our data set is not extensive enough to extend the ephemeris back to the 1980–1982 discovery data.

9. Ultraviolet Amplitudes

To analyze the HST data for the pulsation time variability, we first integrated the observed spectra into one bin, by summing over all wavelengths, to obtain the highest signal to noise ratio. We then transformed the time base to Barycentric Julian Dynamical Time (BJDD), and calculated the Fourier transform of the intensity versus time. For all three stars we conclude that the ultraviolet (HST) data sets showed only the pulsation modes previously detected at optical wavelengths.

9.1. G226–29

Figure 12 shows the Fourier spectra of the light curve of G226–29, converted to amplitude, and the effects of subtracting, in succession, the three pulsations we have detected. The periods used in the subtraction are those of our new ephemeris, but the phases and amplitudes were calculated with a linear least squares fit to the HST data by itself. The residual after this process is probably due to imperfect “pre-whitening” and does not indicate the presence of other pulsations.

The complex spectral windows arises from the fact that the beat period between the pulsations is around 17 hr, and the length of each run of HST was about 3 hr. We can identify the two largest

modes, marked P_1 and P_2 in Figure 12, at 109.08 and 109.47 s, but the central peak, which has a smaller amplitude, is largely hidden in the complex spectral window. The Fourier transform shows that we cannot totally separate the smallest amplitude pulsation, called P_0 , from the two largest amplitude pulsations, called P_1 and P_2 modes; its amplitude and phase have large uncertainties in the HST data set. Note that we use the periods measured in the optical to subtract the light curves (prewhitening), as they are much more accurate than the HST values. The fact that the subtraction works confirms that the optical periods are the same as the ones found in the UV.

After concluding the the ultraviolet (HST) data sets presents only the pulsation modes previously detected, we integrated the observed spectra in 50 Å bins. After determining that the pulsations at all wavelengths were in phase, we fitted three sinusoids simultaneously to each wavelength bin, with phases fixed to the values obtained from the co-added spectra. Figure 13 shows the measured amplitudes. We then normalized the amplitude of the pulsations by their amplitude at 5500 Å to compare with the theoretical models. We used the zeroth order data set to check the amplitude at U, which has similar wavelength, and noticed that, unlike any other observation of the star, the ratio of amplitudes between modes P_1 and P_2 changed significantly, making the use of the UBV_R measurements unreliable, as they were not simultaneous with the HST data. We therefore renormalized the optical data using the amplitude ratios derived from the zeroth order data, assuming its effective wavelength is $3400 \text{ Å} \pm 100 \text{ Å}$. The published transmission curve for the zeroth order data, convolved with the models, would demand an amplitude of pulsation much larger than observed. The ultraviolet efficiency of the mirror must be much lower than measured on the ground, but the effective wavelength is consistent with our measurements, to within our uncertainty of around 100 Å. Even though the central wavelength of the mirror is uncertain, the amplitude vs. wavelength changes only by a few percent over 100 Å, so we include the uncertainty in the wavelength as an uncertainty in the normalization. We note that the observed ultraviolet amplitudes were used to test this effective wavelength and not only are they consistent with it, they exclude any effective wavelength shorter than 3100 Å, as it would produce a much higher amplitude than observed. Note that to calculate $A(\lambda)/A(\lambda_{\text{ref}})$ we only need one amplitude, $A(\lambda_{\text{ref}})$, for normalization [see equation (1)]. By using the Zeroth order

amplitude, we do not need the UBVR amplitudes.

The original HST data set consists of 764 useful pixels from 1180 Å to 2508 Å, each with a width of 1.74 Å, but we can only measure reliable amplitudes for the bins redder than 1266 Å. We convolved the theoretical amplitude spectra (Figure 1) with the measurements summed into 50 Å bins, over the ultraviolet, and the UBVR transmission curves for the optical, obtaining amplitudes directly comparable to the normalized measurements (Table 2).

We then proceeded with a least-squares fit of the amplitude vs. wavelength observed curves to the theoretical ones, and for G226–29 modes P_1 and P_2 fit an $\ell = 1$ g-mode, as shown in Figure 14, and fail to fit the other modes shown. The central mode, P_0 , fits $\ell = 1$ best, but the data are too noisy to exclude $\ell = 2$.

We determined the ℓ , T_{eff} , and $\log g$ independently for each of three modes, P_0 , P_1 and P_2 , by fitting $\text{Amp}(\lambda)/\text{Amp}(5500\text{Å})$ for each periodicity to the model grid, with ℓ , T_{eff} and $\log g$ as free parameters, by least squares. Each mode can be fitted by $\ell = 1$ or $\ell = 2$ with different T_{eff} and $\log g$, but all modes fit only one model, with $T_{\text{eff}} = 11\,750 \pm 20$ K and $\log g = 8.23 \pm 0.06$, for $\ell = 1$. Note that the quoted uncertainties are only those of the least-squares fit and do not represent the true uncertainties. There are substantial systematic errors introduced by the normalization of the flux at 3400 Å, the HST flux calibration, as well as the uncertainties due to the mixing-length approximation used in the model atmospheres (Bergeron et al. 1995, Koester & Vauclair 1997, Koester & Allard 2000), which is incapable of representing the true convection in the star at different depths (Wesemael et al. 1991, Ludwig, Jordan & Steffan 1994).

9.2. G185–32

For G185–32 a fit of the change in pulsation amplitude with wavelength (Table 3) with all three parameters: T_{eff} , $\log g$ and ℓ free resulted in ℓ being consistent with either 1 or 2, but the required temperatures and gravities for $\ell = 2$, $T_{\text{eff}} = 13\,250$ K and $\log g = 8.75$ (Figure 15) were inconsistent with those derived from the time-averaged spectrum itself $T_{\text{eff}} = 11\,750$ K

and $\log g = 8.0$. We therefore fixed the temperature and gravity to those derived using the time-averaged spectra, V magnitude and parallax (Koester & Allard 2000) and fitted the amplitude variation for ℓ . $\ell = 1$ is the best fit for all the modes, except the 141 s mode of G185–32 that does not fit any pulsation index, because its amplitude does not change significantly in the ultraviolet (Figure 16), in contradiction to what is expected from the theoretical models for a DAV. As for G226–29, and PG1351+489, our normalization uses the amplitude of the Zeroth order data because it has the same Fourier spectral window as the ultraviolet data.

9.3. PG1351+489

For PG1351+489, a fit of the normalized ultraviolet amplitudes to the theoretical ones, for the main periodicity at 489 s and its harmonic at 245 s, fit an $\ell = 1$ mode, with $T_{\text{eff}} = 22\,500\text{ K} \pm 250\text{ K}$, and $\log g = 8.0 \pm 0.10$, or an $\ell = 2$ mode with $T_{\text{eff}} = 23100\text{ K} \pm 250\text{ K}$ and $\log g = 7.5 \pm 0.10$. Figure 17 shows that the amplitude ratios are dependent on $\log g$, but again the temperature and $\log g$ determination cannot be untangled. As the optical spectra of Beauchamp et al. (1999) indicate $\log g = 7.9$ for PG1351+489, and $\log g \simeq 8.0$ for the whole DBV class, we conclude that the best solution is $\ell = 1$ and $\log g \simeq 8.0$.

It is important to note that all pulsations have the same phase at all wavelengths, to within the measurement error of a few seconds, and therefore no phase shift with wavelength is detected, assuring that all geometric and some non-adiabatic effects are negligible; the main non-adiabatic effect is a phase shift between the motions (velocities) and the flux variation, not measurable in our data.

10. Discussion

For a DAV, an $\ell = 1$ mode with 109 s period requires a $k = 1$ radial index from pulsation calculations, and therefore the model for G226–29 has to have a thick hydrogen surface layer, around $10^{-4}M_{\star}$ (Bradley 1998). The star may have a thick hydrogen layer as well. The effective

temperature derived from the pulsation amplitudes, $T_{\text{eff}} = 11750$, and surface gravity $\log g = 8.23$, indicate a mass of $(0.75 \pm 0.04)M_{\odot}$, according to the evolutionary models of Wood (1992). As all three modes fit $\ell = 1$, they must be a triplet from a rotationally split $\ell = 1$ mode.

Even though the Bergeron et al. (1995) ML2/ $\alpha = 0.6$ instability strip runs $12460 \text{ K} \geq T_{\text{eff}} \geq 11160 \text{ K}$, we know by comparison of its spectra with other ZZ Cetus that G226–29 is at the blue edge. As it is at the blue edge, such a low temperature indicates the instability strip is at much lower temperature than previously quoted. Also, the observed low amplitude of the pulsations, their short period and the small number of pulsations all indicate it is at the blue edge for its mass, and the higher than average mass suggests a higher temperature instability strip. According to Bradley & Winget (1994), the ML3 instability strip for a $0.75 M_{\odot}$ white dwarf is at 13 100 K, 330K hotter than for a $0.6 M_{\odot}$ star. Giovannini et al. (1998) show that the observed instability strip does depend on mass, as Bradley & Winget (1994) predicted. One of the problems with the determination of an effective temperature for a star is that it may vary with the wavelength used in the determination; even though the effective temperature is a bolometric parameter, none of our observations are. The problem is dramatic for stars with surface convection layers, because of the effects of turbulent pressure on the photosphere. None of the model atmospheres calculated with mixing length theory can reproduce the physical non-local processes involved (Canuto & Dubovikov 1998), requiring different parameterizations at different depths (Ludwig, Jordan & Steffen 1994), and a fine tuning of the convection mixing length coefficient for the wavelength region of interest (Bergeron et al. 1995, Koester & Vauclair 1997, Koester & Allard 2000). The model atmospheres used assume the atmosphere is in hydrostatic and thermodynamical equilibrium, an assumption that must be examined because the timescale for convection is of the same order of the timescale for pulsation.

The periodicity at 141 s for G185–32 does not change its amplitude significantly with wavelength and therefore does not fit any theoretical model. As its period is twice that of the 70.92 s periodicity, one must consider if it is only a pulse shape effect on the 70.92 s periodicity, but normally a pulse shape effect occurs as an harmonic, not a sub-harmonic, because it normally

affects the rise and fall of the pulse. We have no plausible explanation for this periodicity, showing that these stars still have much to teach us.

The periodicity at 560 s rises slowly to the ultraviolet, but as the HST data sets are short, its amplitude has a large uncertainty due to aliasing, as shown by the phase change from ultraviolet (-1.5 ± 8.2 s) to zeroth order data (44.8 ± 9.6 s).

Another surprise for G185–32 is the identification of the periodicities at 70.93 s and 72.56 s as $\ell = 1$ modes. The pulsation models are consistent with such short period $\ell = 1$, $k=1$ mode only for a total mass around $1 M_{\odot}$. Higher k values require even larger mass. But the mass determination from our time average spectra, as well the mass determinations by Koester & Allard (2000) using the IUE spectra plus V mag and parallax, or the optical spectra of Bergeron et al. (1995) all derive a normal mass around $0.56 M_{\odot}$. One possibility to resolve such difference is if the observed modes were a rotationally split $k=0$ mode, but that would require that G185–32 be a binary star, to account for the center of mass changes during pulsation. As G185–32 is not a known binary star, such explanation requires the discovery of a companion, possibly with a high signal-to-noise red spectra.

The models, while useful, clearly lack some of the pulsation physics present in the star.

The splitting of the 70.93 to 72.56 s periodicities, assuming they are m-splitting of the same k and ℓ mode, imply a rotation period around 26 min, but that of the 299.95 s to 301.46 s periodicities would imply a rotation period of 9.7 hr. In the estimate we used

$$P_{\text{rot}} = \frac{1 - C_{kl}^I}{\Delta f}$$

where Δf is the frequency splitting, and used $C_{kl}^I \simeq 0.47$ to 0.48 for $k=1$, $\ell = 1$. The asymptotic value for C_{kl}^I is 0.5, for $k \gg 1$. Either value for the rotation period is much shorter than for normal ZZ Ceti stars (around 1 day) so we must also consider the possibility that the 141 s periodicity, which does not follow the g-mode theoretical prediction, and is harmonically related to the 70.93 s periodicity, must arise from some other cause. The 141 s periodicity of G185–32 is a periodic brightness change that is not accompanied by a change in color, suggesting some kind of geometric

effect.

We are thankful to Bob Williams, the former Director of the STScI for granting us director's discretionary time for the project, to Jeffrey Hayes, our project scientist at STScI, for the continuous help with the HST data reduction and to Bill Welsh, from the University of Texas, for bringing the zeroth order data to our attention. Support for this work was provided by NASA through grants number GO-5581, GO-6011 and GO-6442 from the Space Telescope Science Institute, which is operated by AURA, Inc., under NASA contract NAS5-26555, Support to S.O.K. was also provided by CNPq-Brazil. D.K. acknowledges financial support for work on HST observations from the DLR through grant No. 50 OR 96173. Jiang acknowledges financial support from Chinese Natural Science Foundation, grant No. 19673008.

Table 1: Optical Amplitudes for G226–29

Color	Amp_1	Amp_0	Amp_2
U	1.61 ± 0.09	2.87 ± 0.09	3.25 ± 0.09
B	1.53 ± 0.06	2.66 ± 0.06	2.86 ± 0.06
V	1.27 ± 0.08	2.30 ± 0.08	2.28 ± 0.08
R	1.00 ± 0.10	1.81 ± 0.10	1.94 ± 0.10

Table 2: Measured Amplitudes in mma for G226–29

λ_{ef}	Amp ₀	Amp ₁	Amp ₂
1266	20.58 ± 4.44	26.20 ± 4.56	43.53 ± 4.56
1315	12.52 ± 2.25	24.26 ± 2.31	36.18 ± 2.31
1364	11.56 ± 1.79	22.04 ± 1.83	33.15 ± 1.83
1412	10.48 ± 1.47	20.02 ± 1.51	26.05 ± 1.51
1461	7.76 ± 1.15	15.78 ± 1.18	22.69 ± 1.18
1510	7.61 ± 1.22	15.33 ± 1.25	20.20 ± 1.25
1559	7.52 ± 1.24	14.29 ± 1.27	19.96 ± 1.27
1607	6.01 ± 1.00	13.98 ± 1.03	21.01 ± 1.03
1656	4.95 ± 0.79	9.42 ± 0.81	13.56 ± 0.81
1705	4.04 ± 0.76	9.98 ± 0.78	11.59 ± 0.77
1753	4.04 ± 0.73	8.42 ± 0.75	10.62 ± 0.75
1802	4.27 ± 0.68	6.27 ± 0.69	10.16 ± 0.69
1851	3.38 ± 0.65	6.00 ± 0.66	9.78 ± 0.66
1899	3.33 ± 0.66	7.40 ± 0.68	9.23 ± 0.68
1948	3.48 ± 0.60	6.01 ± 0.62	8.10 ± 0.62
1997	4.15 ± 0.60	6.08 ± 0.62	8.90 ± 0.62
2046	3.42 ± 0.56	4.80 ± 0.57	8.98 ± 0.57
2094	2.06 ± 0.54	5.84 ± 0.55	7.96 ± 0.55
2143	2.38 ± 0.46	5.46 ± 0.48	6.88 ± 0.48
2192	2.98 ± 0.48	5.42 ± 0.49	7.49 ± 0.49
2240	1.90 ± 0.47	5.14 ± 0.48	7.49 ± 0.48
2289	1.87 ± 0.40	4.93 ± 0.41	6.66 ± 0.41
2338	1.92 ± 0.39	4.81 ± 0.40	6.38 ± 0.40
2386	1.61 ± 0.39	3.94 ± 0.40	6.80 ± 0.40
2435	1.25 ± 0.36	3.98 ± 0.36	6.18 ± 0.36
2484	2.19 ± 0.42	4.02 ± 0.43	6.36 ± 0.43
3400	1.22 ± 0.32	2.72 ± 0.32	3.70 ± 0.32

Table 3: Amplitudes for G185–32

Ultraviolet			Zeroth Order	
Period (s)	Amplitude (mma)	Time of maxima (s)	Amplitude (mma)	Time of maxima (s)
215.7	7.81 ± 0.34	61.7 ± 1.6	2.68 ± 0.15	61.8 ± 2.0
370.1	4.66 ± 0.36	106.1 ± 4.5	2.15 ± 0.16	99.6 ± 4.3
70.9	4.48 ± 0.36	29.8 ± 0.9	1.81 ± 0.17	28.5 ± 1.0
72.5	3.18 ± 0.36	26.6 ± 1.3	1.21 ± 0.16	21.4 ± 1.6
301.3	4.22 ± 0.36	25.1 ± 4.1	1.90 ± 0.16	289.0 ± 4.0
300.0	4.14 ± 0.36	182.8 ± 4.1	1.86 ± 0.16	199.6 ± 4.1
560.0	3.37 ± 0.36	44.8 ± 9.6	1.74 ± 0.16	558.5 ± 8.2
141.8	1.85 ± 0.37	98.3 ± 4.5	1.56 ± 0.16	103.2 ± 2.3

REFERENCES

- Allard N.F., Koester D., Feautrier N., Spielfiedel A. 1994, *A&A. Suppl.* 108, 417
- Beauchamp, A., Wesemael, F., Bergeron, P., Fontaine, G., Saffer, R., Liebert, J., & Brassard, P. 1999, *ApJ*, 516, 887.
- Bergeron, P., Saffer, R.A. & Libert, J. 1992, *ApJ*, 394, 228.
- Bergeron, P., Wesemael, F., Lamontagne, R., Fontaine, G., Saffer, R.A., & Allard, N.F. 1995, *ApJ*, 449, 258
- Bradley, P.A. 1998, *Baltic Astronomy*, 7, 111
- Bradley, P. & Winget, D.E. 1994, *ApJ*, 421, 236.
- Canuto, V.M. & Dubovikov, M. 1998, *ApJ*, 493, 834
- Chabrier, G., Ashcroft, N.W., & de Witt, H.E. 1992, *Nature*, 360, 48.
- Eracleous, M. & Horne, K. 1996, *ApJ*, 471, 427
- Finley, D. S., Koester, D., Basri, G. 1997, *ApJ*, 488, 375
- Fontaine, G., Brassard, P. Bergeron, P. & Wesemael, F. 1992, *ApJ*, 399, L91
- Fontaine, G., Brassard, P., Wesemael, F. & Tassoul, M. 1994, *ApJ*, 428, L61
- Fontaine, G., Brassard, P., Bergeron, P. & Wesemael, F. 1996, *ApJ*, 469, 320.
- Harrington, R.S., Dahn, C.C. 1980, *AJ*, 85,454
- Giovannini, O., Kepler, S. O., Kanaan, A., Wood, M.A., Claver, C. F., Koester, D. 1998, *Baltic Astronomy*, 7, 131.
- Kepler, S.O., & Nelan, E.P. 1993, *AJ*, 105, 608

- Kepler, S.O., Robinson, E.L. & Nather, R.E. 1983, *ApJ*, 271, 744
- Kepler, S.O., Robinson, E.L. & Nather, R.E. 1995, *Calibrating Hubble Space Telescope: Post Servicing Mission*, ed. A. Koratkar & C. Leitherer, Space Telescope Science Institute, Baltimore, p. 104
- Kepler S.O., Giovannini O., Wood M.A., Nather R.E., Winget D.E., Kanaan A., Kleinman S.J., Bradley P.A., Provencal J.L., Clemens J.C., Claver C.F., Watson T.K., Yanagida K., Krisciunas K., Marar T.M.K., Seetha S., Ashoka B.N., Leibowitz E., Mendelson H., Mazeh T., Moskalik P., Krzesiński J., Pajdosz G., Zoła S., Solheim J.-E., Emanuelsen P.-I., Dolez N., Vauclair G., Chevreton M., Fremy J.-R., Barstow M. A., Sansom A.E., Tweedy R.W, Wickramasinghe D.T., Ferrario L., Sullivan D.J., van der Peet A.J., Buckley D.A.H., and Chen A.-L. 1995a, *ApJ*, 447, 874
- Kepler, S.O., Giovannini, O., Kanaan, A., Wood, M.A., & Claver, C.F. 1995b, *Baltic Astronomy*, 4, 221
- Koester, D., & Allard, N.F. 1993, in "White Dwarfs: Advances in Observation and Theory", ed. M.A. Barstow, NATO ASI Series 403, p.237.
- Koester, D., & Allard, N.F. 2000, *Baltic Astronomy*, in press.
- Koester, D., Allard, N.F., & Vauclair, G. 1994, *A&A*, 291, L9.
- Koester, D., Allard, N.F., & Vauclair, G. 1995, in *Proc. of the 9th European Workshop on White Dwarfs*, ed. D. Koester & K. Werner, (Berlin:Springer-Verlag), p. 196.
- Koester, D., Schulz, H. & Weidemann, V. 1979, *A&A*, 76, 262.
- Koester, D., & Vauclair, G. 1997, in *Proceedings of the 10th European Workshop on White Dwarfs*, ed. Jordi Isern, M. Hernanz & E. Garcia-Berro, NATO ASI Series, Springer, Berlin, p. 429.
- Ludwig, H.-G., Jordan, S. & Steffen, M. 1994, *A&A*, 284, 105.

- McGraw, J.T., & Fontaine, G. 1980, unpublished results.
- McGraw, J.T., Fontaine, G. Lacombe, P., Dearborn, D.S.P., Gustafson, J., Starrfield, S.G. 1981, *ApJ*, 250, 349.
- Robinson, E. L., Kepler, S. O. & Nather, R. E. 1982, *ApJ*, 259, 219.
- Robinson, E.L., Mailloux, T.M., Zhang, E., Koester, D., Stiening, R.F., Bless, R.C., Percival, J.W., Taylor, M.J. & van Citters, G.W. 1995, *ApJ*, 438, 908.
- Segretain, L., Chabrier, G., Hernanz, M., Garcia-Berro, E., Isern, J., & Mochkovitch, R. 1994, *ApJ*, 434, 641.
- Vauclair, G., Schmidt, H., Koester, D., & Allard, N. 1997, *A&A*, 325, 1055.
- Wesemael, F., Bergeron, P., Fontaine, G. & Lamontagne, R. 1991, in *White Dwarfs*, eds. G. Vauclair & E.M. Sion, NATO ASI Series, 336, 159.
- Winget, D.E., Hansen, C.J., Liebert, J., Van Horn, H.M., Fontaine, G., Nather, R.E., Kepler, S.O., & Lamb, D.Q. 1987, *ApJ*, 315, L77.
- Winget, D. E., Kepler, S. O., Kanaan, A., Montgomery, M. H., Giovannini, O. 1997, *ApJ*, 487, L191.
- Winget, D.E., Nather, R.E & Hill, J.A. 1987, *ApJ*, 316, 305.
- Wood, M. A. 1992, *ApJ*, 386, 539.
- Wood, M. A. 1995, in Proc. of the 9th European Workshop on White Dwarfs, ed. D. Koester & K. Werner, (Berlin:Springer-Verlag), p.41.

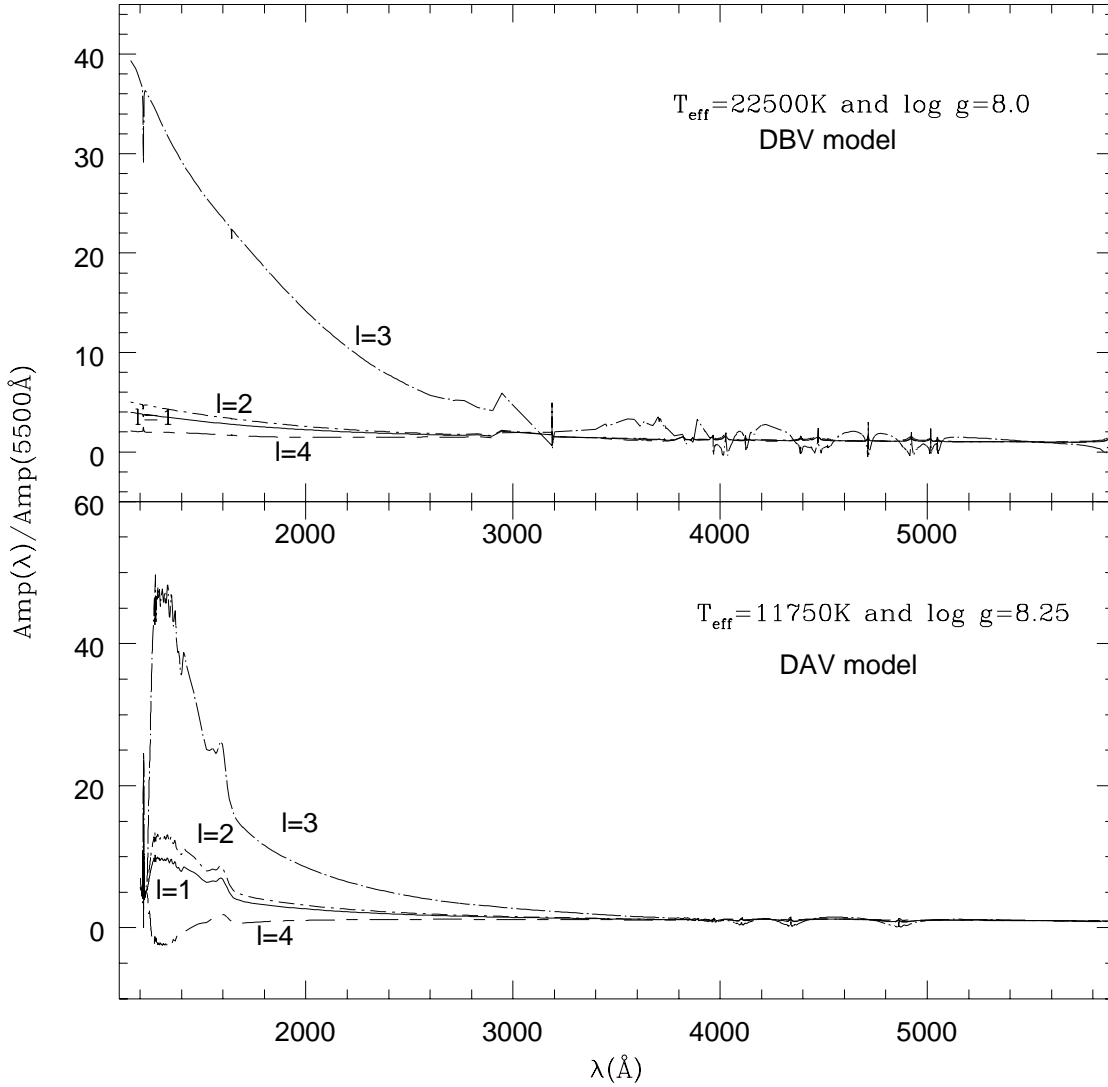


Fig. 1.— The amplitudes of the $\ell = 1$ to $\ell = 4$ pulsation modes as a function of wavelength for DA and DB models. These amplitudes, for different values of T_{eff} and $\log g$ were calculated from the most recent version of the model atmosphere code by Koester (Finley, Koester & Basri 1997).

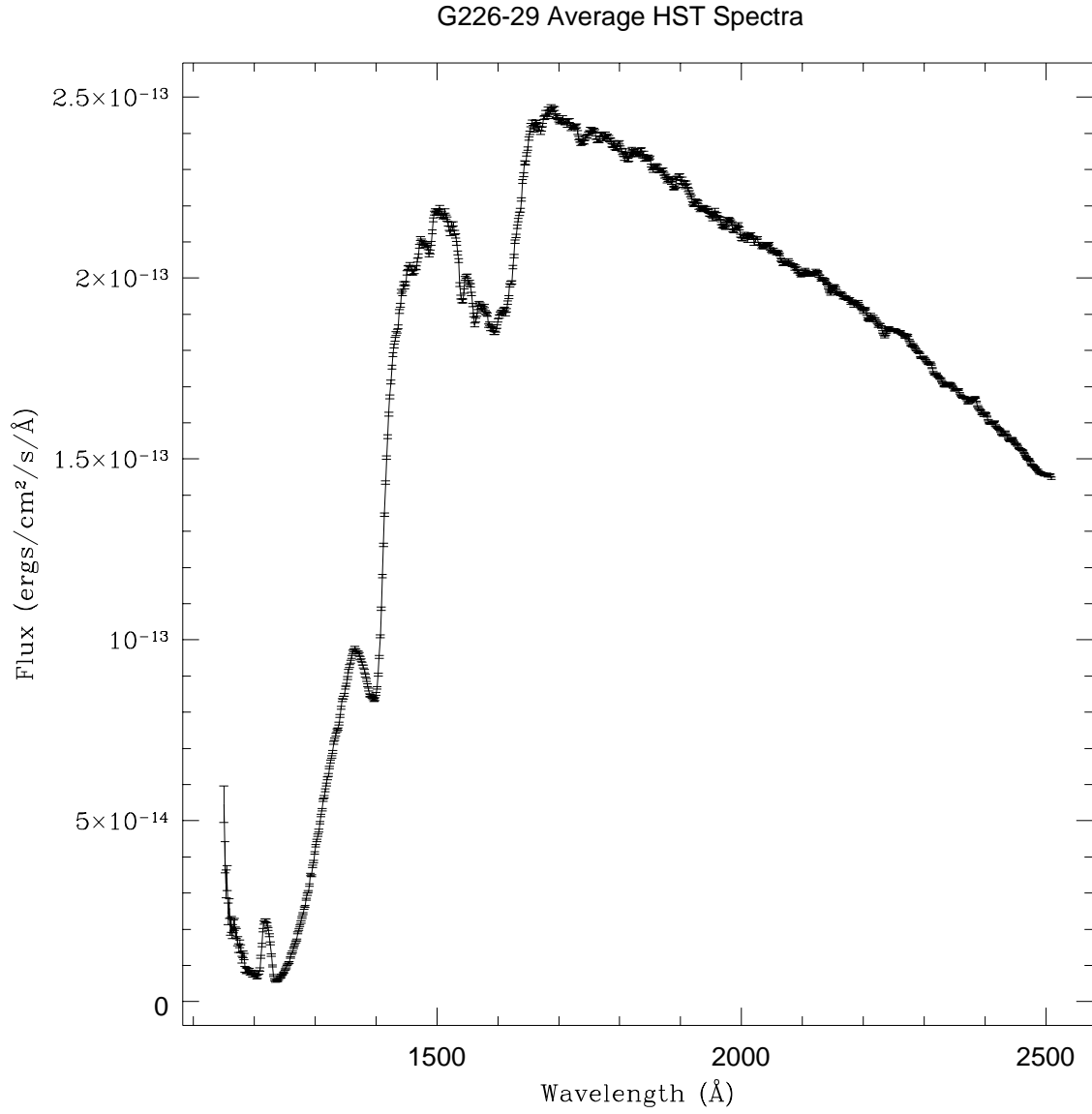


Fig. 2.— Average FOS spectrum of the pulsating DA white dwarf G226-29, after re-calibration.

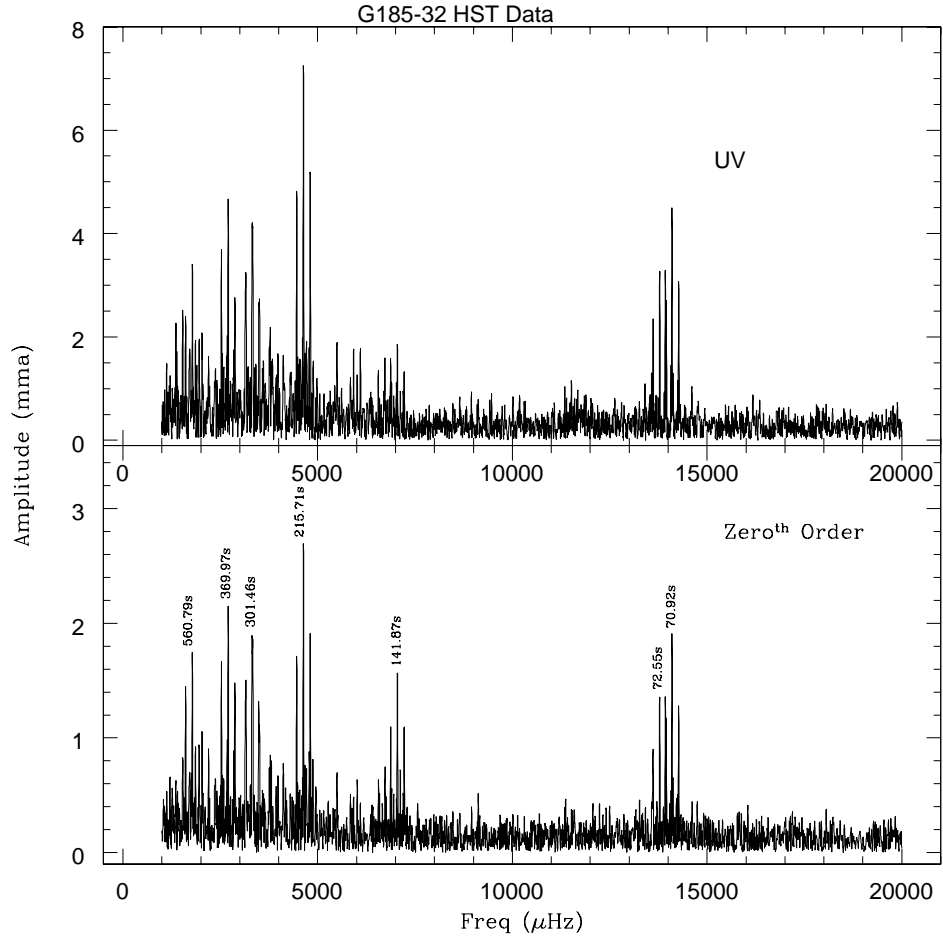


Fig. 3.— Fourier transform of the UV (upper panel) and Zeroth Order (lower panel) data for G185–32. The peaks not annotated are artifacts introduced by gaps in the data (aliasing).

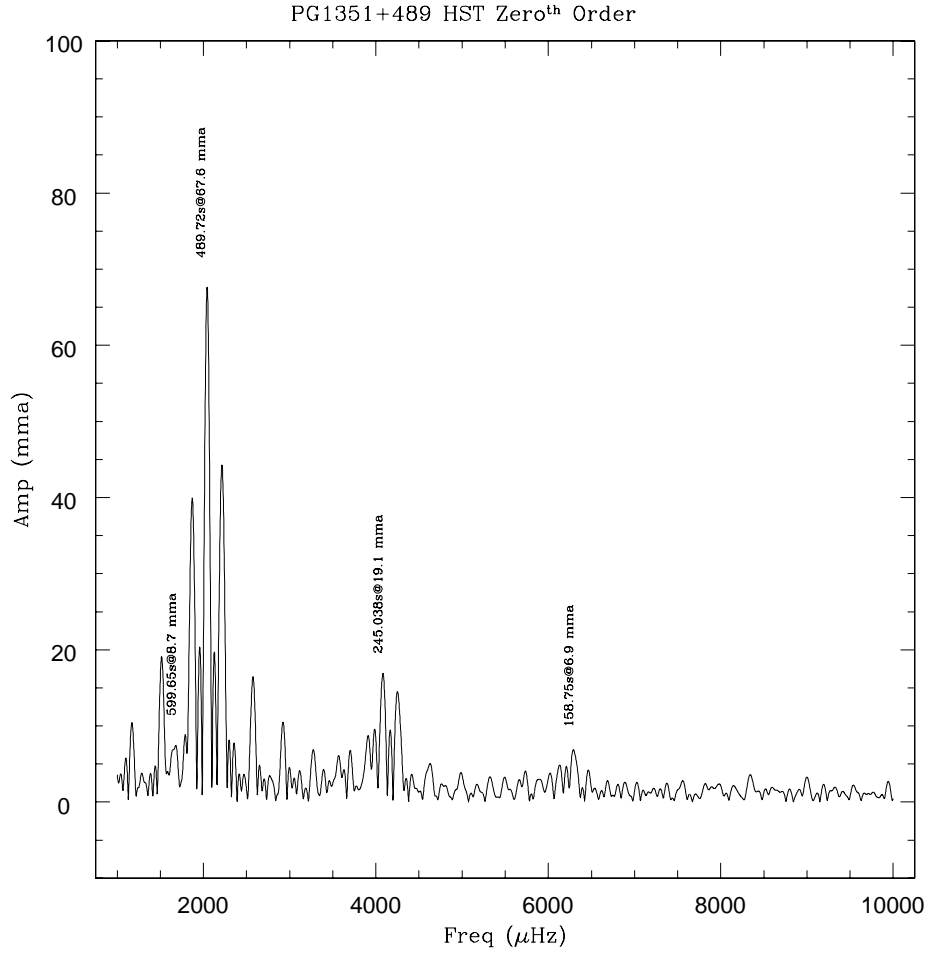


Fig. 4.— Fourier transform of the Zeroth Order data for PG1351+489 showing the 489 s and 245 s periodicities. The peak at 158.75 s is only marginally significant. The peak at 599.65 s has an amplitude of 8.7 mma on the Zeroth Order data, which corresponds to $4.3 \langle amp \rangle$ and therefore is significant.

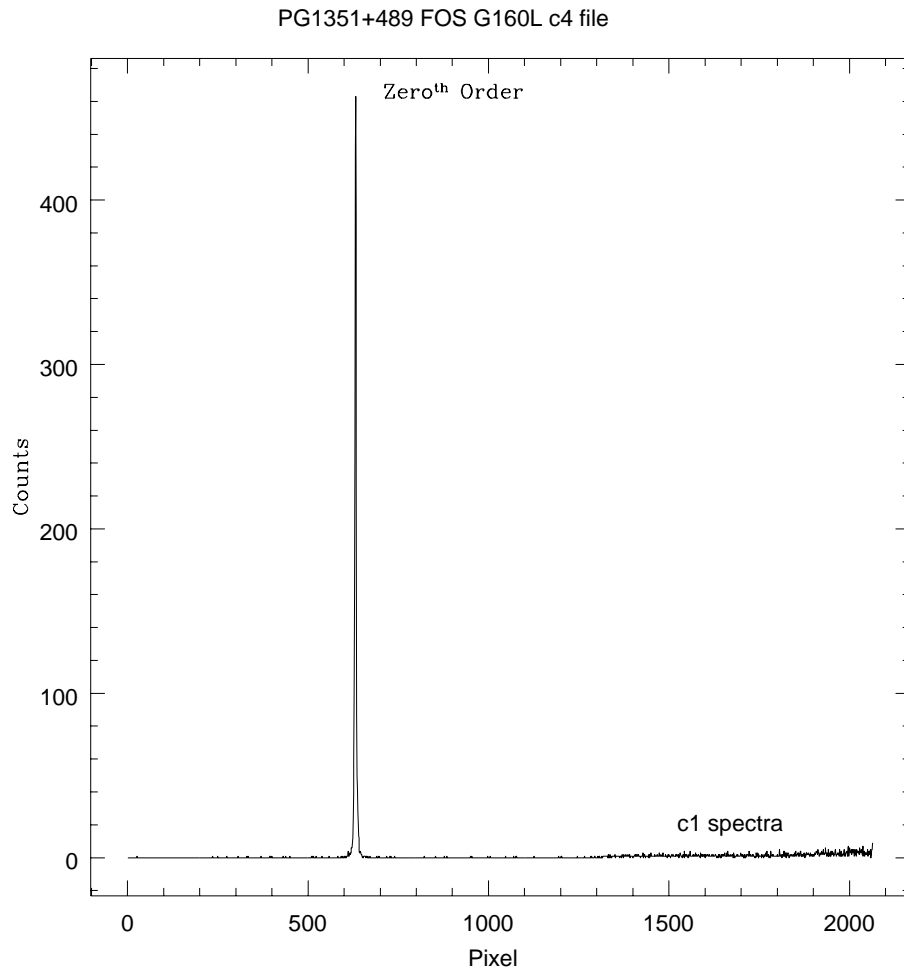


Fig. 5.— Placement and count rate of the Zeroth order data, the undiffracted image of the target object.

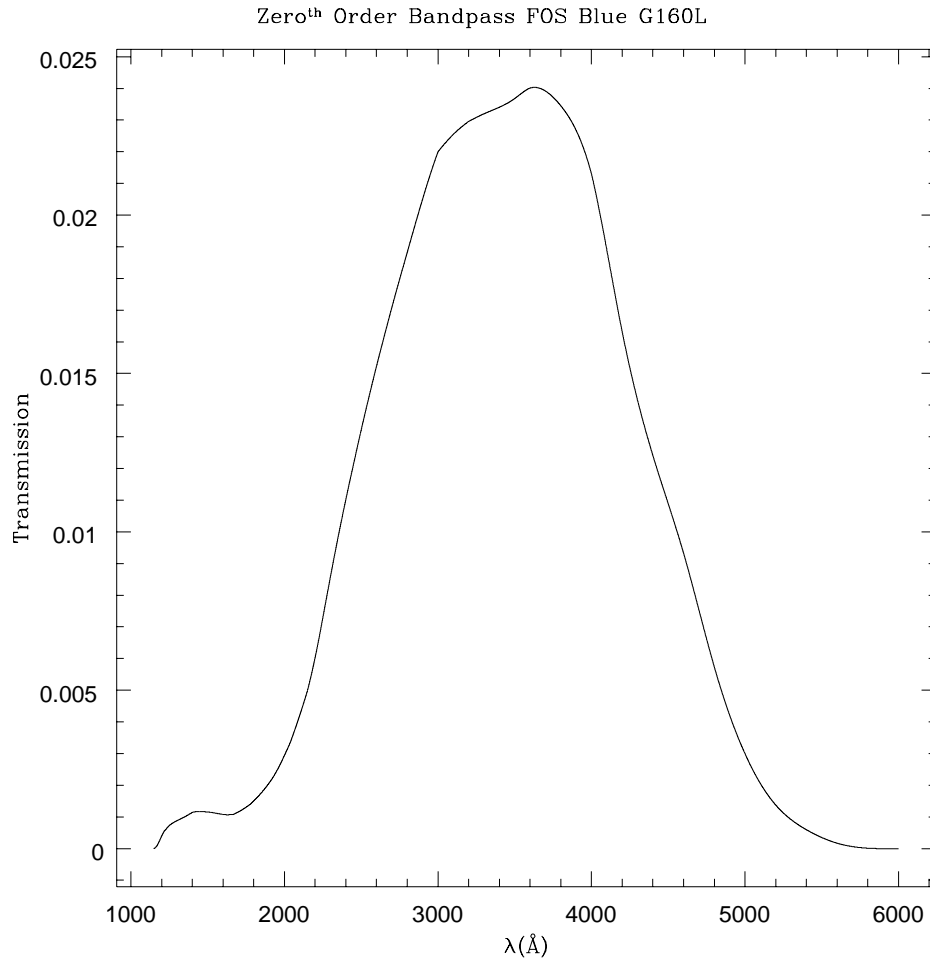


Fig. 6.— Band pass for the Zeroth data as measured on the ground prior to installation of the FOS on HST.

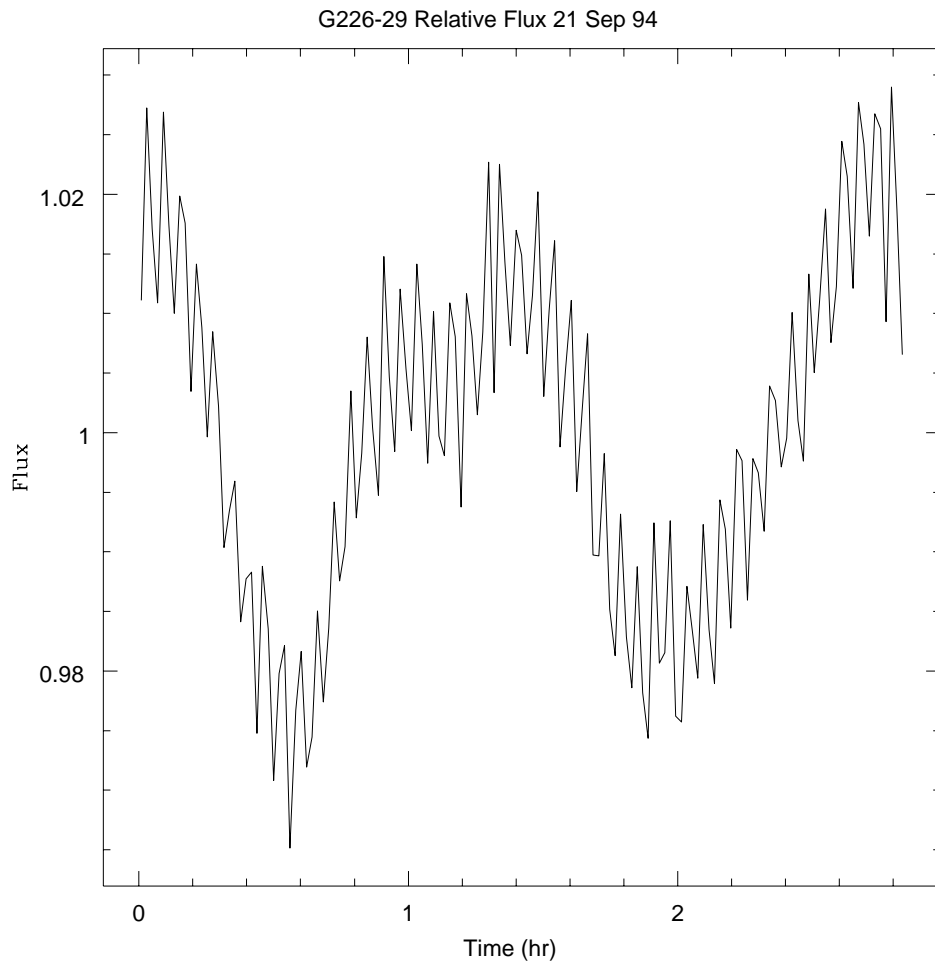


Fig. 7.— Light loss with the 1.0 arcsec aperture. In this figure we plot the count rate summed through all wavelengths, divided by the average, versus time. The rapid variation on a time scale of 100 sec is caused by the pulsations of the star.

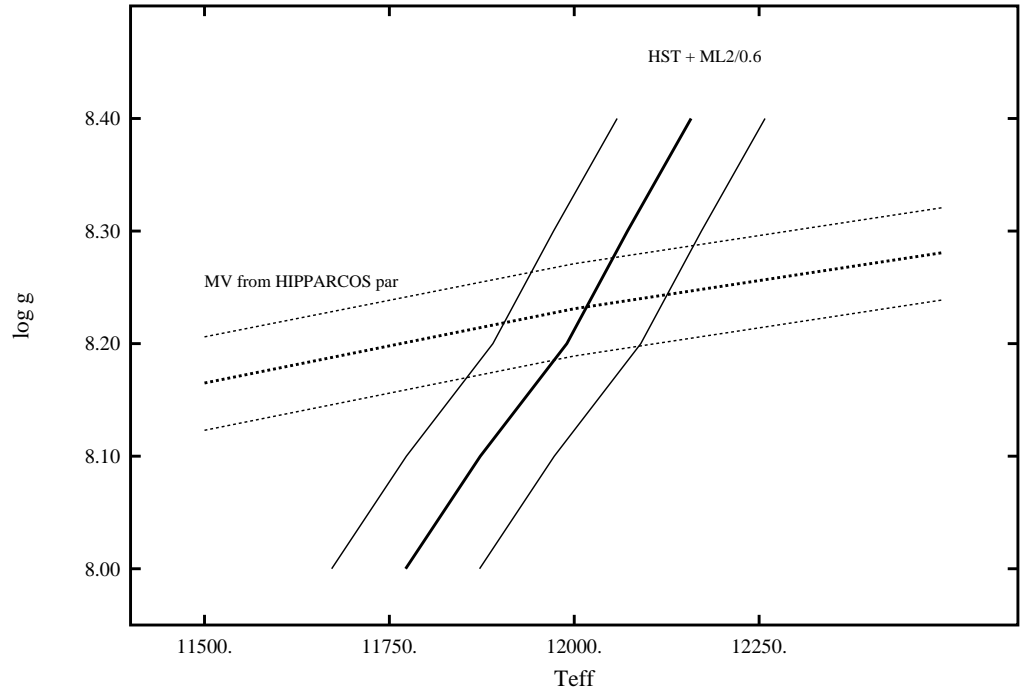


Fig. 8.— Temperature and $\log g$ determination for G226-29 using the spectra itself and HIPPARCOS parallax. The heavy line shows the determination of T_{eff} and $\log g$ from the spectra, and their uncertainties. The dotted lines the constraints imposed by the HIPPARCOS parallax.

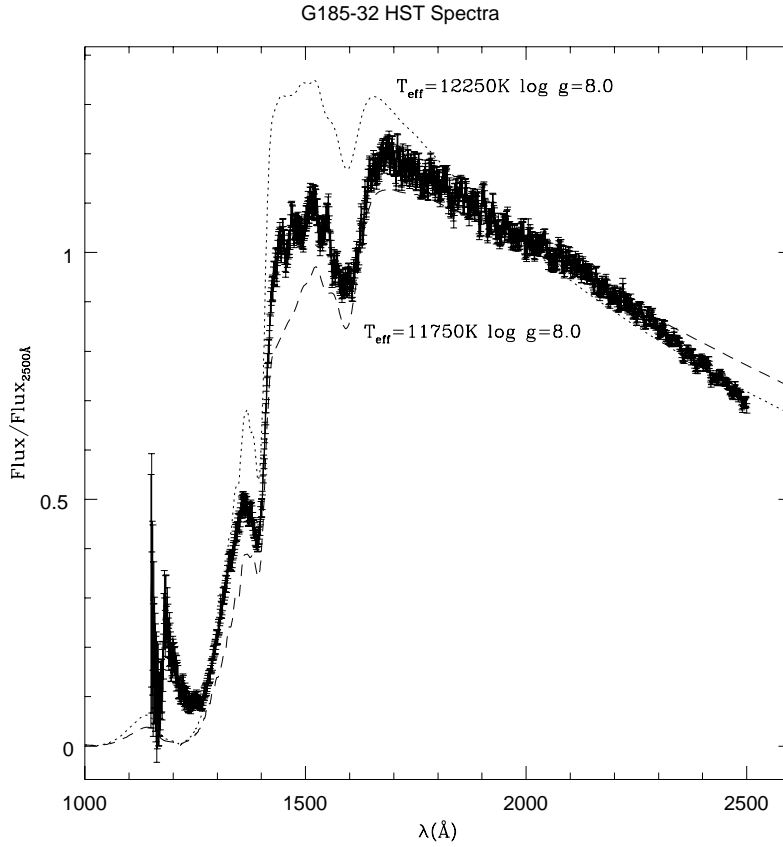


Fig. 9.— Ultraviolet spectra for G185–32, with 1σ error-bars. For displaying purposes, we have normalized the spectra at 2000Å , as the bump on the observed spectrum is due to inadequate flux calibration of the FOS. The dotted line represent model with $\log g = 8.0$ and $T_{\text{eff}} = 12250\text{ K}$, and the dashed line $T_{\text{eff}} = 11750\text{ K}$.

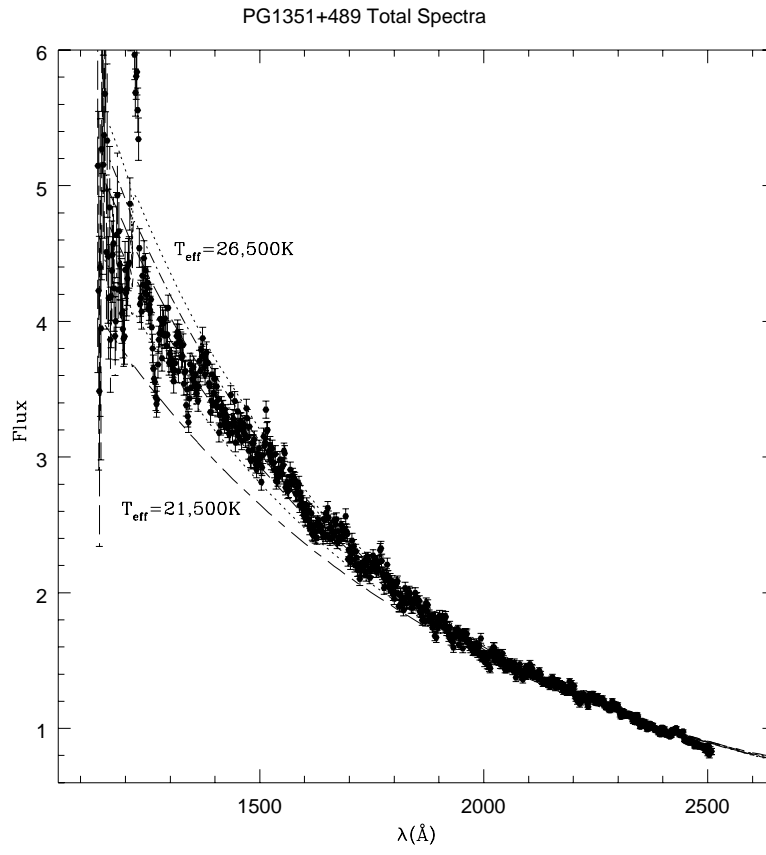


Fig. 10.— Ultraviolet spectra for PG1351+489. The lines represent models with fixed $\log g = 8.0$ and different temperatures.

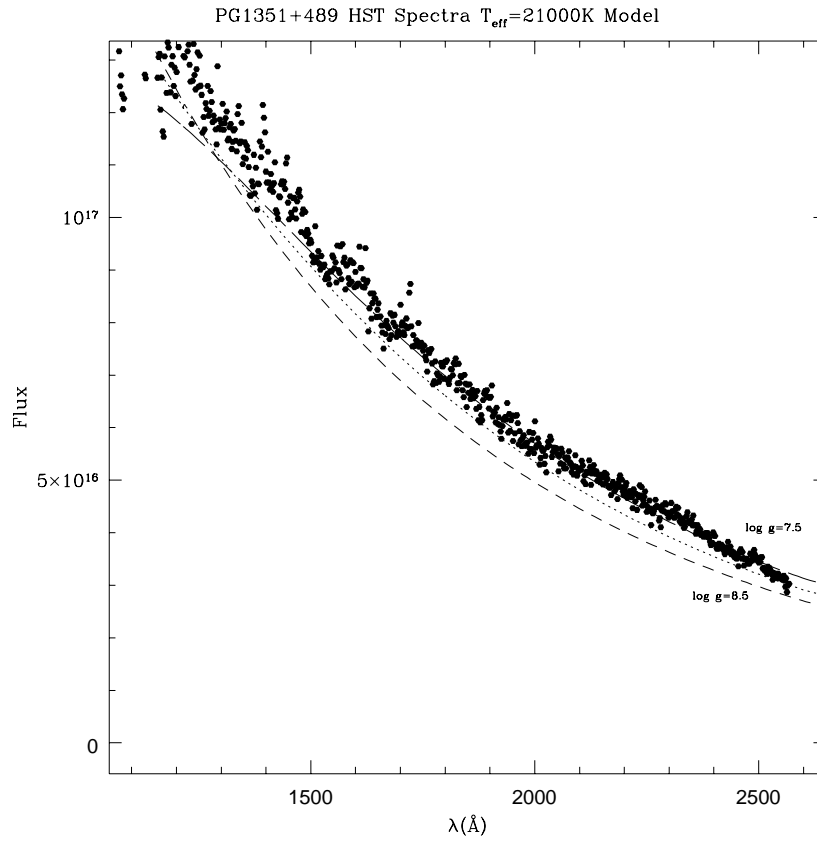


Fig. 11.— Flux change due to changes in $\log g$ for DB models showing the spectra itself is not very sensitive to surface gravity.

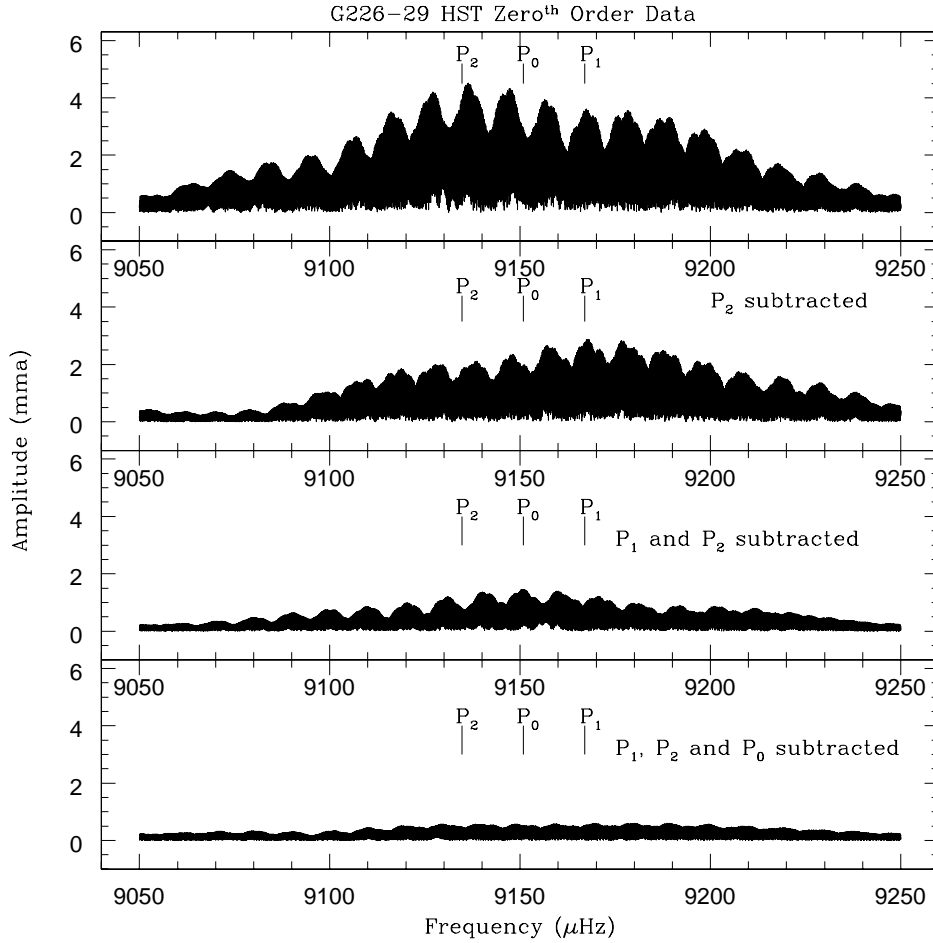


Fig. 12.— Fourier amplitude spectra of the HST data set. The second panel shows the amplitude spectra after we subtracted the periodicity P_2 from the light curve (prewhitening). The lower panel shows the amplitude spectra after we subtracted from the light curve all three periodicities P_1 , P_2 and P_2 . The leftover power corresponds to P_0 .

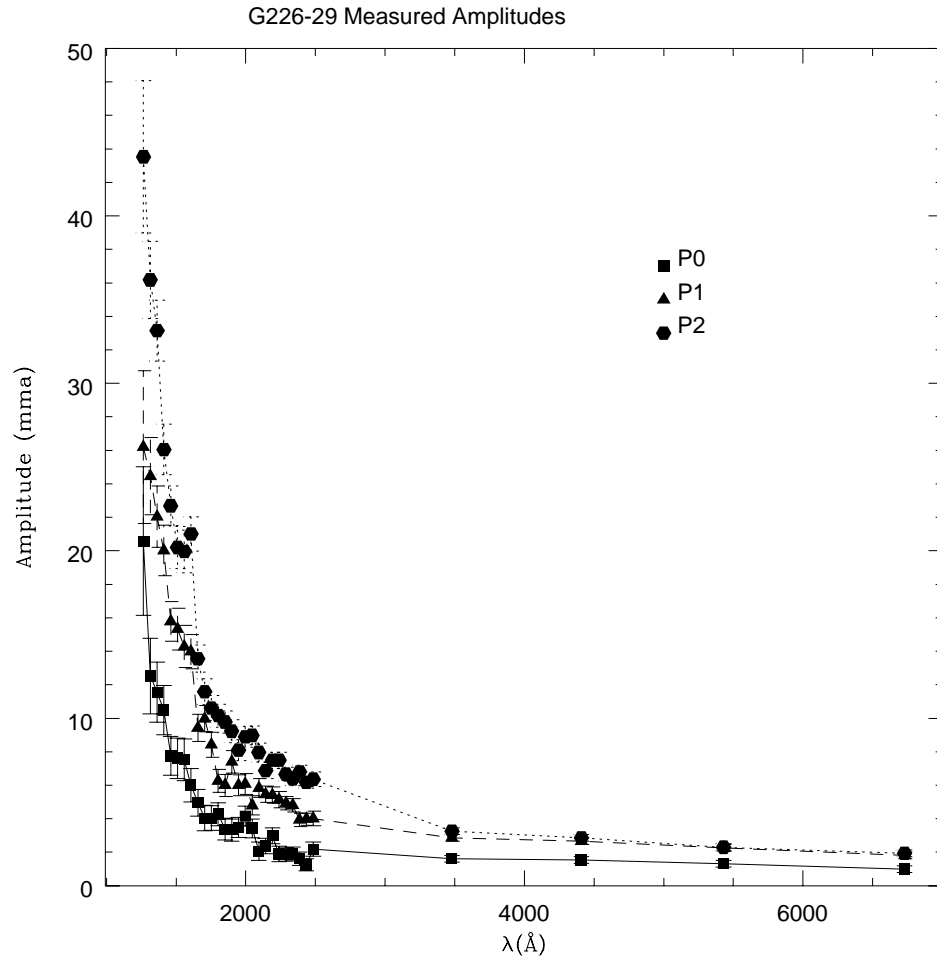


Fig. 13.— Measured Amplitudes for the three modes of G226-29. The lines simply connect the observations, to guide the eye.

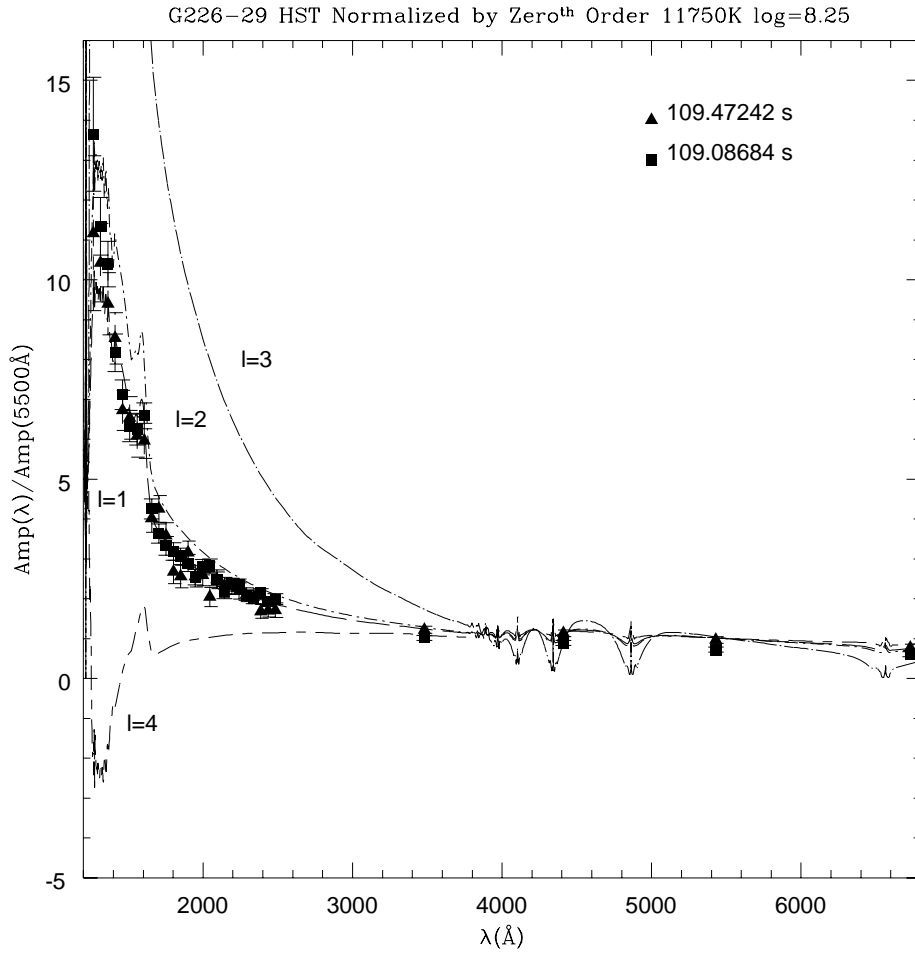


Fig. 14.— The amplitudes of the $\ell = 1$ to $\ell = 4$ pulsation modes in a pulsating DA white dwarf as a function of wavelength. The points are the measured amplitudes of the two main periodicities of G229-29.

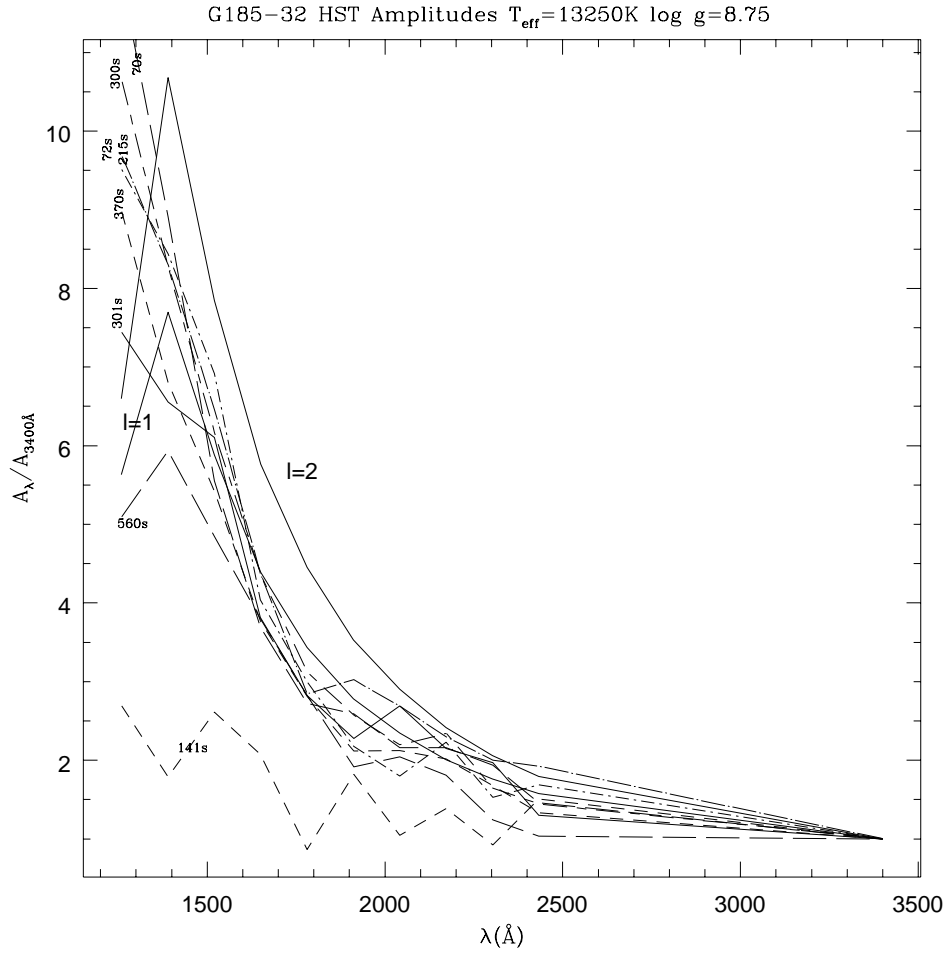


Fig. 15.— Comparison of the model amplitudes (solid lines) with the data for G185–32, when we allow T_{eff} , $\log g$ and ℓ vary. The 141 s periodicity does not rise towards the UV, indicating it is not caused by a g-mode pulsation.

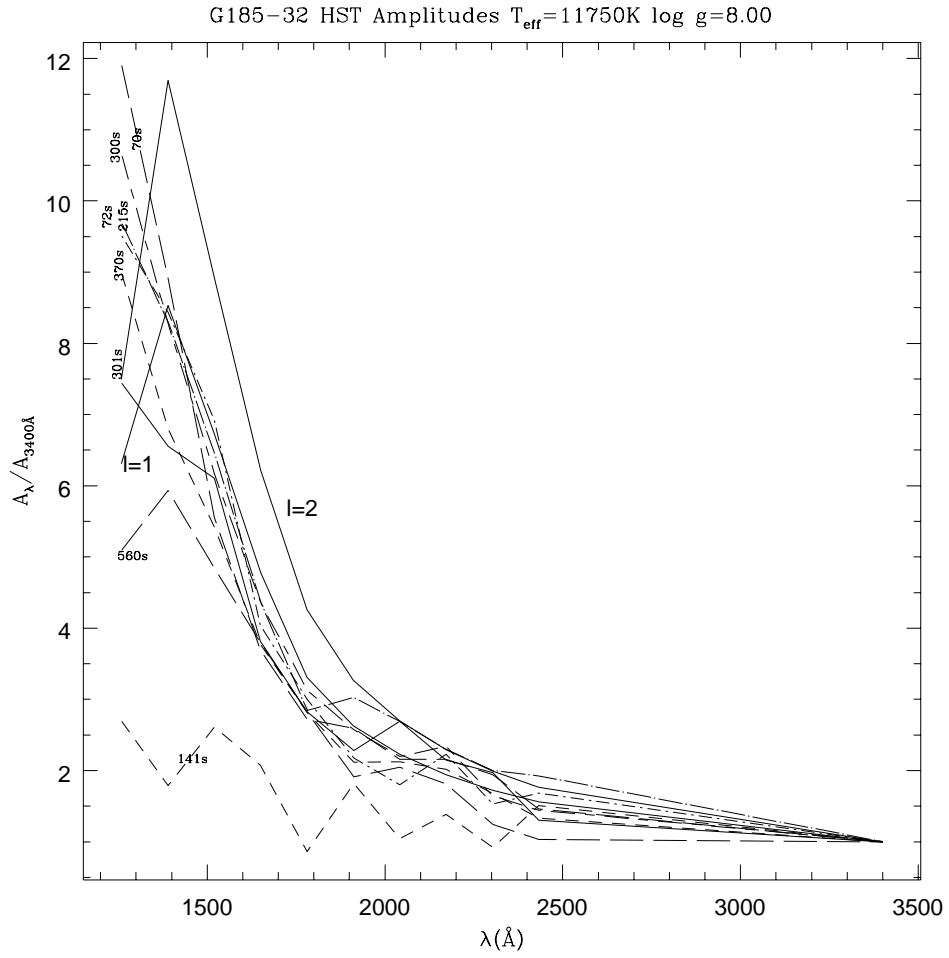


Fig. 16.— Comparison of the model amplitudes (solid lines) with the data for G185–32, when we fix the $T_{\text{eff}} = 11\,750$ K and $\log g = 8.0$, consistent with the optical and UV spectra, V and parallax.

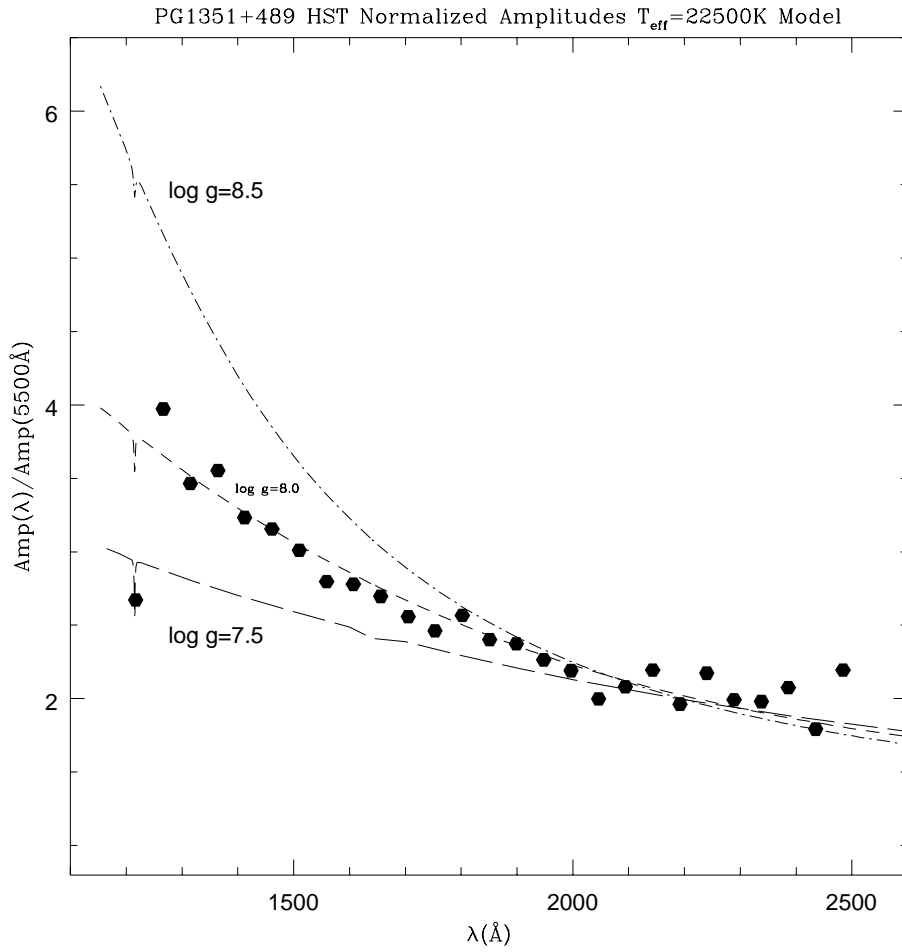


Fig. 17.— Amplitude change due to changes in $\log g$ for DB models. The lines represent the normalized amplitudes expected for models with fixed $T_{\text{eff}} = 22\,500$ K and different values for $\log g$. Even though the spectra are not very sensitive to surface gravity, the amplitudes are.